Size-dependent Electrochemical Metal Growth Kinetics

Harikrishnan N. Nambiar and Francis P. Zamborini*

Department of Chemistry, University of Louisville, Louisville, Kentucky 40292, United States

*Corresponding Author

Email: f.zamborini@louisville.edu

ABSTRACT

This work explores the electrochemical deposition (ECD) of Au onto chemically preformed Au nanoparticles (NPs) as a function of Au NP size. The growth potential and current depend strongly on the size of the preformed Au NPs (seeds) due to different Au NP size-dependent kinetics of the growth process. Electrochemical reversibility depends on the Au NP size, scan rate, metal precursor concentration ($[AuCl_4^-]$), and Au NP coverage. The Au NPs need to reach a critical total surface area in order to have enough active area to cause the ECD over the entire electrode to be electrochemically reversible and operate under linear diffusion mass transfer-limited conditions. The smaller Au NPs require less total surface area to reach this condition because they have higher activity per surface area, which is not fully understood but could be due to a greater percentage of defects on their surface, such as edge and corner atom sites.

INTRODUCTION

Electrochemical deposition (ECD) involves the reduction of simple metal ions or metal complexes to the metallic form onto a conductive electrode surface. It is widely used for coating purposes[1] with applications in electronics,[2] catalysis,[3] Raman detection,[4] and sensing.[5] ECD can

also be used to form arrays of metal and alloy nanoparticles (NPs)[6, 7] of various size and shape on electrode surfaces.[8-10] For example Glasscott *et. al.* used droplet mediated size-selective ECD to form ligand-free, uniformly distributed Pt NPs on an amorphous graphite electrode.[6] This was achieved by confining the precursor metal salt to a water droplet suspended in oil. Ivanova and Zamborini used ECD to prepare different sized Au NPs by the controlling the deposition potential, where the Au NPs oxidized at more negative potentials as the size decreased.[11] Others have performed metal ECD in various templates, such as porous membranes,[12] the step edges of highly-oriented pyrolytic graphite (HOPG),[13] or lithographically-defined templates,[14] to prepare one-dimensional metal nanorods and nanowires.

ECD traditionally occurs by the well-known nucleation and growth mechanism, where the formation of a supercritical (or stable) nucleus of metal atoms (or clusters) occurs first at an overpotential.[15-17] These nuclei then grow larger at a lower overpotential (more positive potential) by catalyzing the reduction of metal ions or complexes onto the nucleus, known as the growth step. Metal ion (or complex) reduction to form the initial nucleation sites has a higher activation energy, hence requires higher overpotential, compared to the continued growth of the formed nucleation sites.[18] The growth step is the basis for the chemical seed-mediated growth of metal nanostructures, where pre-formed metal NPs act as nucleation sites, or "seeds", for further growth of the seeds into larger metal nanostructures of controlled shape and size.[19] Abdelmoti and Zamborini adopted the chemical seed-mediated growth method to synthesize Au nanorods (NRs) by an electrochemical seed-mediated deposition process in the presence of cetyltrimethylammonium bromide (CTAB).[20]

Numerous studies have been conducted to understand the nucleation and growth phenomenon of metal ECD on various electrode materials.[16, 21, 22] For example, Ustarroz *et al.*

showed that the early stages of Pt electrochemical growth on carbon substrates may be affected by the aggregation, self-alignment and partial coalescence of nanoclusters ~2 nm in diameter.[23] Pesika and co-workers showed that by tuning the ECD of Ag on an Ag electrode within the reaction-controlled regime, where the current increases exponentially with applied overpotential, the island nucleation density can be systematically varied and thin films with varied roughness can be formed.[24] Macpherson and co-workers used identical location scanning transmission electron microscopy to visualize the very early stages of nucleation at the single atom level, which involved potential-induced atom movement, atom clustering, and cluster transformation into crystalline NPs.[25] Penner and co-workers discovered that the metal ECD rate affects the particle size dispersion in an ensemble of NPs.[26] Slow growth on an array of NPs with no diffusional coupling present between neighboring NPs on the electrode surface greatly reduces the particle size-dispersion.[26] There has been a great deal of work measuring the overpotential needed to induce nucleation on various electrode surfaces and using ECD as a tool to create metallic nanostructures on electrode surfaces, but little attention has been given to the growth step kinetics in ECD.

EXPERIMENTAL SECTION

Chemicals and Materials. $HAuCl_4 \cdot 3H_2O$ was synthesized from 99.9% metallic Au. Acetone (Pharmaco-AAPER, ACS/USP grade), ethanol (Pharmaco-AAPER, ACS/USP grade) and 2-propanol (Sigma Aldrich, ACS reagent) were used as solvents for cleaning indium-tin-oxide (ITO) - coated glass electrodes (CG-50IN-CUV, R_s = 8-12 Ω). ITO-coated glass slides were purchased from Delta Technologies Limited (Loveland, CO). Sodium borohydride (Sigma Aldrich, ≥ 98.5 reagent grade), trisodium citrate salt (Bio-Rad laboratories), perchloric acid (Merck, 60%) and

hydrogen peroxide solution (Sigma Aldrich, 30% wt) were used as received. NANOpure ultrapure water (Barnstead, resistivity = 18.2 mΩ cm) was used for all aqueous solutions.

Chemical Synthesis of Citrate-Stabilized Au NPs. Citrate-stabilized 4 nm, 15 nm, and 50 nm average diameter Au NPs were synthesized by well-established literature methods[1-3] described by our group previously and confirmed by electron microscopy as well as UV-vis spectroscopy.[4] The methods involve borohydride reduction of $AuCl_4^-$ in the case of 4 nm diameter Au NPs, citrate reduction of $AuCl_4^-$ at boiling temperature in the case of 15 nm diameter Au NPs, and seed-mediated reduction of $AuCl_4^-$ at 15 nm Au NP seeds with hydrogen peroxide in the case of 50 nm diameter Au NPs. The final concentrations of $AuCl_4^-$ used for the 4 nm, 15 nm, and 50 nm diameter Au NPs were 0.25 mM, 0.25 mM, and 0.085 mM, respectively.

Au NP Size Characterization. Au NP size confirmation was achieved by anodic stripping voltammetry (ASV) of Au NPs attached to a glass/ITO electrode by electrophoretic deposition (EPD). The potential was scanned from -0.2 V to 1.2 V in 0.01 M KBr plus 0.1 M $KClO_4$ solution, where the Au oxidation peak potential provides information about the Au NP size.[4-6] The Au NP size was also confirmed by UV-vis spectroscopy and scanning electron microscopy (SEM) as described in our previous work.[4]

Electrophoretic Deposition (EPD) of Au NPs onto Glass/ITO. We used the procedure described by Allen *et al.* for the hydroquinone (HQ)-mediated electrophoretic deposition (EPD)[5] of all Au NP sizes directly on glass/ITO electrodes. The three-electrode setup consisted of a cleaned glass/ITO working electrode (area = 0.84 cm^2), Pt wire counter electrode, and Ag/AgCl (3 M KCl) reference electrode connected to a CH Instruments (Austin, TX) 660E electrochemical workstation[5, 7] and placed in a beaker cell with the electrodes spaced approximately 1.5 cm from each other in a triangle arrangement. The conductive side of the glass/ITO working electrode

faced toward the reference and counter electrodes. For the EPD of 4 nm diameter Au NPs, the beaker cell contained 24 mL of nanopure water, 1 mL of as-prepared Au NPs and 5 mL of 0.1 M HQ. The EPD of 15 nm diameter Au NPs was performed in a solution containing 21 mL of nanopure water, 4 mL of as-prepared Au NPs and 5 mL of 0.1 M HQ. The EPD solution for 50 nm diameter Au NPs contained 27.5 mL of Au NPs and 2.5 mL of 0.2 M HQ. The total volume of the EPD solution was 30 mL in all cases. The final concentrations of Au for 4 nm, 15 nm, and 50 nm Au NP EPD solutions were 8.33 μM, 33.3 μM, and 77.9 μM, respectively, and HQ was 16.7 mM in all cases. An electrode potential of 1 V, 1.2 V and 2.2 V, respectively, for 4 nm, 15 nm, and 50 nm diameter Au NPs was applied to the glass/ITO working electrode and held for 90 s for 4 nm, 30 s for 15 nm, and 120 s for 50 nm diameter Au NPs. These conditions lead to different sized Au NPs with the same total surface area (~4 x 10^{-6} C). After EPD, the glass/ITO electrode was removed from the beaker cell and rinsed immediately with copious amount of nanopure water before drying under a stream of N_2. The concentration of EPD solution and EPD time are changed accordingly to achieve variable Au NP coverage. After EPD, all glass/ITO/Au NP electrodes were placed in an ozone cleaner for 8 minutes in order to remove any stabilizer or impurities from the Au NP surfaces.

Electrochemical Surface Area Characterization. A three-electrode set-up consisting of the ozone-cleaned glass/ITO/Au NPs working electrode, Pt wire counter electrode, and an Ag/AgCl (3M KCl) reference electrode was used for Au NP electrochemical surface area characterization. Cyclic voltammograms (CVs) were obtained in 0.1 M $HClO_4$ solution by scanning from 0.0 V to 1.4 V and back at a scan rate of 100 mV/s. Integration of the Au oxide reduction peak near 0.8 V on the return segment provided information about the total surface area of the Au NPs, allowing determination of the surface area and coverage for the different-sized Au NPs.[4]

Electrochemical Deposition (ECD) Experiments. The three-electrode electrochemical cell consisted of a glass/ITO working electrode with and without the different-sized Au NPs, Pt wire counter electrode, and an Ag/AgCl (3M KCl) reference electrode. The ECD was performed in a solution of 0.001 M or 0.0001 M $HAuCl_4.3H_2O$ in 0.1 M $KClO_4$ solution in a beaker cell using linear sweep voltammetry (LSV) from 1.0 V to 0.0 V at a scan rate of 100, 10, 1 and 0.1 mV/s.

Electron Microscopy Characterization. Scanning Electron Microscopy (SEM) images of glass/ITO/Au NPs were obtained with a Thermo-Fisher Scientific Apreo C LoVac field emission scanning electron microscope (FESEM) operating at an accelerating voltage of 20.0 kV using an in-lens Trinity T1 Detector.

RESULTS AND DISCUSSION

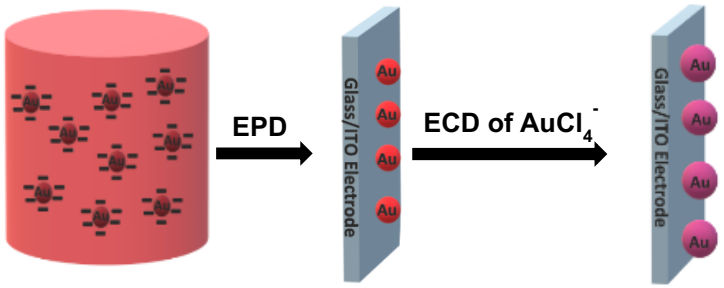

Scheme 1. General experimental design involved in the ECD experiments.

Experimental Design. In this paper we examine the ECD of Au onto chemically preformed Au NPs of varied size attached to indium tin oxide-coated glass (glass/ITO) electrodes. Scheme 1 shows the general experimental design of this work. Step 1 of Scheme 1 involves the electrophoretic deposition (EPD) of different sized, chemically-preformed citrate-stabilized Au nanoparticles (NPs) onto a glass/ITO working electrode using our previously developed hydroquinone (HQ)-mediated method.[27, 28] The size of the Au NPs was controlled through chemical synthesis (4 nm, 15 nm, and 50 nm) while the coverage of Au NPs on the glass/ITO

electrode was controlled by the EPD deposition conditions (Au NP concentration, deposition time, and deposition potential). After the EPD step, we measured the total surface area of the deposited Au NPs (Figure 1A) by measuring the charge of the reduction peak after running an oxidation/reduction cycle from 0.0 V to 1.4 V in 0.1 M $HClO_4$.[29] Step 2 of Scheme 1 involves the electrochemical deposition (ECD) of Au onto the glass/ITO/Au NP electrodes in 0.001 M $HAuCl_4 \cdot 3H_2O$ and 0.1 M $KClO_4$ by sweeping the potential from 1.0 V to 0.0 V vs Ag/AgCl (3 M KCl) at varied scan rates. The peak potential and peak current provide kinetic and thermodynamic information about the ECD of Au onto the different-sized preformed Au NP nucleation sites (metal growth step).

ECD as a Function of Au NP Size with Constant Total Au Surface Area. Figure 1 shows linear sweep voltammograms (LSVs) of Au ECD on glass/ITO and glass/ITO/Au NP electrodes with different size Au NPs at different scan rates, including 100 mV/s (Figure 1B), 10 mV/s (Figure 1C), 1 mV/s (Figure 1D) and 0.1 mV/s (Figure 1E). The main cathodic peak in the LSVs ranging from about 0.80 to 0.25 V is due to the electrochemical reduction of $AuCl_4^-$ to metallic Au^0 at the glass/ITO and glass/ITO/Au NP surfaces according to the following electrochemical reaction:

$$AuCl_4^- + 3e^- \rightarrow Au^0 + 4Cl^- \quad E^0 = 808 \text{ mV vs. Ag/AgCl (3 M KCl)} \quad (1)$$

The electrochemical reduction of $AuCl_4^-$ on bare glass/ITO (black legend in Figure 1B), at a scan rate of 100 mV/s, occurs at a peak potential of 268 ± 19 mV, which corresponds to the formation of Au nucleation sites at the bare glass/ITO electrode surface. Au nucleation on bare glass/ITO does not start until an overpotential of about ~640 mV, which is required to overcome the activation barrier for the initial reduction of $AuCl_4^-$ to form Au^0 nucleation sites on the glass/ITO surface.[30] The $AuCl_4^-$ reduction to form Au_x^0 nucleation sites (small meal clusters) is a high

activation energy process that requires more negative potential than required for $AuCl_4^-$ reduction onto Au_x metal clusters (or Au seed NPs).[15, 31]

$$xAuCl_4^- + (3x)e^- \rightarrow Au_x^0 + (4x)Cl^- \quad \text{(nucleation = high activation energy = high overpotential)} \quad (2)$$

$$yAuCl_4^- + (3y)e^- + Au_x^0 \rightarrow Au_{x+y}^0 + (4y)Cl^- \quad \text{(growth = low activation energy = low overpotential)} \quad (3)$$

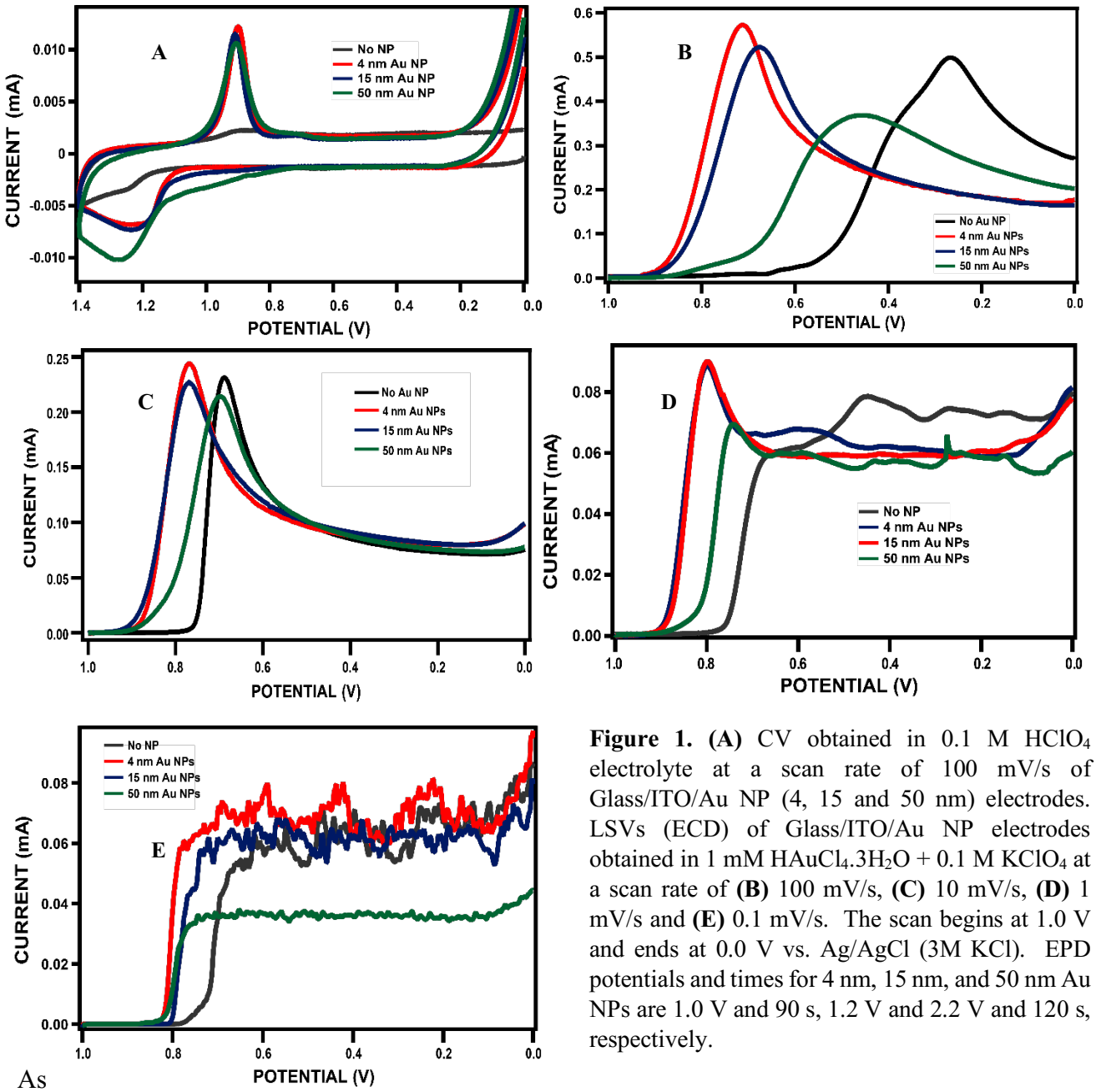

Figure 1. (A) CV obtained in 0.1 M $HClO_4$ electrolyte at a scan rate of 100 mV/s of Glass/ITO/Au NP (4, 15 and 50 nm) electrodes. LSVs (ECD) of Glass/ITO/Au NP electrodes obtained in 1 mM $HAuCl_4.3H_2O$ + 0.1 M $KClO_4$ at a scan rate of **(B)** 100 mV/s, **(C)** 10 mV/s, **(D)** 1 mV/s and **(E)** 0.1 mV/s. The scan begins at 1.0 V and ends at 0.0 V vs. Ag/AgCl (3M KCl). EPD potentials and times for 4 nm, 15 nm, and 50 nm Au NPs are 1.0 V and 90 s, 1.2 V and 2.2 V and 120 s, respectively.

As shown in Figure 1B, the presence of preformed Au NPs on the electrode surface catalyzes the

$AuCl_4^-$ reduction, leading to ECD occurring at lower overpotentials for all sized Au NPs, which promotes the growth of the preformed Au NPs into larger Au NPs (equation 3). Hence the peak deposition potential for growth occurs at more positive potentials (equation 3) than that for nucleation on bare glass/ITO (equation 2). With the total Au surface area constant at ~4 x 10^{-6} C for the three different sized Au NPs on the glass/ITO surface, the more positive ECD potential for the 4 nm Au NPs indicates faster charge transfer kinetics. The ECD rate increased with decreasing Au NP size as shown by the more positive growth potential as the size of the Au NPs decreased. The onset potentials for 4 nm, 15 nm, and 50 nm Au NPs at 100 mV/s were 928 ± 4 mV, 914 ± 3 mV, and 868 ± 4 mV, respectively. The peak potentials for 4 nm, 15 nm, and 50 nm Au NPs at 100 mV/s were 702 ± 4 mV, 687 ± 8 mV, and 585 ± 26 mV, respectively. The smaller Au NPs required lower overpotentials compared to the larger Au NPs to initiate the electrochemical reduction of $AuCl_4^-$ and growth of the Au NPs. All sizes exhibit more positive ECD potential than the nucleation peak potential of 268 ± 19 mV on bare glass/ITO. Interestingly, on bare glass/ITO, there are shoulder peaks at ~400 mV and 600 mV, indicating that there may be different sites on the ITO that have different nucleation kinetics.

In addition to the positive shift in reduction potential with decreasing Au NP size, the peak current associated with $AuCl_4^-$ reduction increased with decreasing Au NP size, which was 5.72 x 10^{-4} A, 4.87 x 10^{-4} A and 2.65 x 10^{-4} A, respectively, for the 4 nm, 15 nm, and 50 nm Au NPs, while the peak current due to nucleation and growth at the glass/ITO electrode was 4.72 x 10^{-4} A. Kinetic limitations not only shift the peak potential negative but also decrease the peak current as the electron transfer rate constant decreases with increasing Au NP size and for Au nucleation and growth at bare glass/ITO.[32] We do not believe the different currents are due to different electrode areas since the Au NP surface area of ~4 x 10^{-6} C was kept constant and the peak current should

be proportional to the entire glass/ITO electrode area (0.84 cm^2) since the coverage of Au NPs is well above the nanoparticle spacing required for diffusional overlap (linear diffusion) at the scan rate employed (see Table 1).

Table 1. ECD data for Glass/ITO and Glass/ITO/Au NP (4 nm, 15 nm and 50 nm) electrodes obtained in 1 mM $HAuCl_4 \cdot 3H_2O$ + 0.1 M $KClO_4$ at scan rates of 100 mV/s, 10 mV/s, 1 mV/s and 0.1 mV/s.

Electrode Condition	Scan Rate (mV)	Diffusion Layer Thickness (μm)	Onset Potential (mV)	Peak Potential (mV)	*Peak or ‡Limiting Current (A)	SA Coverage (C)	V Coverage (C)	Au NP Coverage (NP/μm²)	NP Spacing (μm)
Glass/ITO	100	8.94×10^1	647 ± 3	268 ± 19	*4.72 (± 0.16) x 10^{-4}	-	-	-	-
	10	2.83×10^2	788 ± 9	673 ± 21	*2.54 (± 0.21) x 10^{-4}	-	-	-	-
	1	8.94×10^2	801 ± 15	NA	‡5.01 (± 0.42) x 10^{-5}	-	-	-	-
	0.1	2.83×10^3	801 ± 16	NA	‡6.09 (± 0.22) x 10^{-5}	-	-	-	-
Glass/ITO/ 4 nm Au NPs	100	8.94×10^1	928 ± 4	702 ± 4	*5.72 (± 0.69) x 10^{-4}	4.53 (± 0.10) x 10^{-6}	5.66 (± 0.12) x 10^{-6}	52.4 (± 1.1)	0.138
	10	2.83×10^2	931 ± 6	766 ± 8	*2.45 (± 0.11) x 10^{-4}	4.41 (± 0.34) x 10^{-6}	5.52 (± 0.43) x 10^{-6}	51.1 (± 4.0)	0.140
	1	8.94×10^2	933 ± 4	793 ± 6	*9.56 (± 0.74) x 10^{-5}	4.50 (± 0.26) x 10^{-6}	5.63 (± 0.32) x 10^{-6}	52.1 (± 3.0)	0.139
	0.1	2.83×10^3	860 ± 3	NA	‡7.39 (± 0.46) x 10^{-5}	4.31 (± 0.06) x 10^{-6}	5.39 (± 0.07) x 10^{-6}	49.9 (± 0.7)	0.142
Glass/ITO/ 15 nm Au NPs	100	8.94×10^1	914 ± 3	687 ± 8	*4.87 (± 0.52) x 10^{-4}	4.53 (± 0.17) x 10^{-6}	1.62 (± 0.06) x 10^{-5}	2.84 (± 0.11)	0.594
	10	2.83×10^2	929 ± 3	765 ± 8	*2.21 (± 0.08) x 10^{-4}	4.39 (± 0.34) x 10^{-6}	1.57 (± 0.12) x 10^{-5}	2.75 (± 0.21)	0.604
	1	8.94×10^2	933 ± 3	797 ± 2	*8.78 (± 0.55) x 10^{-5}	4.67 (± 0.18) x 10^{-6}	1.67 (± 0.06) x 10^{-5}	2.93 (± 0.11)	0.585
	0.1	2.83×10^3	886 ± 7	NA	‡6.85 (± 0.08) x 10^{-5}	4.38 (± 0.10) x 10^{-6}	1.57 (± 0.04) x 10^{-5}	2.75 (± 0.06)	0.603
Glass/ITO/ 50 nm Au NPs	100	8.94×10^1	868 ± 4	585 ± 26	*2.65 (± 0.66) x 10^{-4}	4.55 (± 0.13) x 10^{-6}	8.26 (± 0.24) x 10^{-5}	0.39 (± 0.01)	1.60
	10	2.83×10^2	885 ± 2	699 ± 11	*2.06 (± 0.06) x 10^{-4}	4.25 (± 0.22) x 10^{-6}	7.73 (± 0.41) x 10^{-5}	0.37 (± 0.02)	1.65

	1	8.94 x 10^2	873 ± 13	746 ± 4	*6.77 (± 0.17) x 10^{-5}	4.49 (± 0.20) x 10^{-6}	8.16 (± 0.36) x 10^{-5}	0.39 (± 0.02)	1.61
	0.1	2.83 x 10^3	852 ± 6	NA	‡4.03 (± 0.48) x 10^{-5}	4.60 (± 0.19) x 10^{-6}	8.37 (± 0.34) x 10^{-5}	0.40 (± 0.02)	1.59

To confirm that the more positive ECD potential at smaller Au NPs is due to faster electron transfer kinetics, we performed ECD of Au onto glass/ITO and glass/ITO/Au NPs at slower scan rates. When the scan rate of the ECD process decreased to 10 mV/s, 1 mV and 0.1 mV/s, as shown in Figures 1C, 1D and 1E, respectively, using the same Au surface area as described earlier, the growth potential shifted positive for all three sized Au NPs and for Au nucleation and growth at the bare glass/ITO. When the scan rates were 10 mV/s and 1 mV/s, the onset and peak growth potentials are identical for 4 nm and 15 nm Au NPs and are just slightly more negative for 50 nm Au NPs and for nucleation and growth at the bare glass/ITO surface. At 0.1 mV/s, the growth onset potential is about the same at ~800 mV for all three sized Au NPs and ~100 mV more negative for bare glass/ITO. Interestingly, the current reaches a steady-state value at 0.1 mV/s and the limiting current is a little smaller for the 50 nm Au NPs, even with a similar growth potential and similar Au surface area coverage. The reason for this behavior is not fully understood. At the slower scan rates diffusional overlap should be even more prevalent, resulting in linear diffusion, peak current proportional to the glass/ITO electrode, and a duck-shaped voltammogram. It is likely that convection becomes important at these very slow scan rates, which would lead to a steady-state limiting current (sigmoidal) rather than the expected duck-shaped voltammogram.

Table 1 shows the peak growth potentials and peak currents for all the electrodes studied with constant Au NP surface area and various scan rates (100, 10, 1.0, and 0.1 mV/s). In all cases the Au NP surface area indicates a coverage that would lead to Au NP-Au NP spacings (Supporting Information) that are significantly shorter than the calculated diffusion layer thickness (Supporting

Information) based on the scan rate and the diffusion coefficient of $AuCl_4^-$ (D_O = 1.00 x 10^{-5} cm^2/s). This would lead to conditions of linear diffusion at an array of electrodes, which would give peak currents proportional to the entire electrode area of 0.84 cm^2. The biggest difference in growth potential occurs at 100 mV/s, indicating that the kinetics for $AuCl_4^-$ are significantly faster at the smallest 4 nm Au NPs. At a scan rate of 10 mV/s, the peak growth potentials are very similar for 4 nm and 15 nm Au NPs at around 766 ± 8 mV and 765 ± 8 mV, respectively, which is close to the thermodynamically expected potential (808 mV). For 50 nm Au NPs, the peak growth potential is shifted slightly to 699 ± 11 mV. As expected, the nucleation and growth at bare glass/ITO has the highest overpotential with a peak potential of 673 ± 21 mV. When the scan rate is 1 mV/s, the onset and peak growth potentials follow similar trends with the 10 mV/s, where the peak growth potentials for 4 nm, 15 nm, and 50 nm Au NPs are 793 ± 6 mV, 797 ± 2 mV, and 746 ± 4 mV, respectively. The onset potentials for 4 nm, 15 nm, and 50 nm Au NPs are 933 ± 4 mV, 933 ± 3 mV, and 873 ± 13 mV, and the onset potential due to nucleation and growth at bare glass/ITO is at 801 ± 15 mV. At an even slower scan rate of 0.1 mV/s the $E_{1/2}$ growth potentials were very similar for 4 nm, 15 nm, and 50 nm Au NPs (~800 mV) as compared to the $E_{1/2}$ for nucleation and growth of ~650 mV, which is still kinetically limited. The peak or limiting currents are also shown in Table 1 for the different sized Au NPs and bare glass/ITO at the different scan rates. The peak current is the highest for the 4 nm Au NPs at 100 mV/s, again due to faster electron transfer kinetics. The peak currents, or limiting currents in some cases, become similar for the 4 nm and 15 nm Au NPs at 10, 1.0 and 0.1 mV/s, but a little lower for the 50 nm Au NPs for reasons that are not fully understood. The limiting current for the bare glass/ITO at 0.1 mV/s is similar to the 4 nm and 15 nm Au NPs as expected since the entire glass/ITO electrode is the same area and

controls the current. The presence of a limiting current could be due to convection at slow scan rates as mentioned earlier.

ECD Under Constant Au NP Coverage Conditions. We also performed ECD of Au on Au NPs at different scan rates while keeping a constant number of Au NPs on the glass/ITO surface (~1 Au NP/μm^2 area of the electrode). This is achieved by maintaining the total SA coverages of 4 nm, 15 nm, and 50 nm Au NPs before ECD (Figure 2A) at 9.49 x 10^{-8} C, 1.58 x 10^{-6} C and 1.41 x 10^{-5} C, respectively (Table S1). At a scan rate of 100 mV/s, the peak growth potentials for 4 nm, 15 nm, and 50 nm Au NPs are 616 ± 3 mV, 638 ± 3 mV, and 650 ± 24 mV, respectively. Under these conditions, the ECD kinetics are more hindered at the smaller 4 nm Au NPs compared to the 15 nm and 50 nm Au NPs. We believe this is due to the lower overall surface area of the 4 nm Au NPs by about a factor of 14 and 156 compared to the 15 and 50 nm Au NPs, respectively.

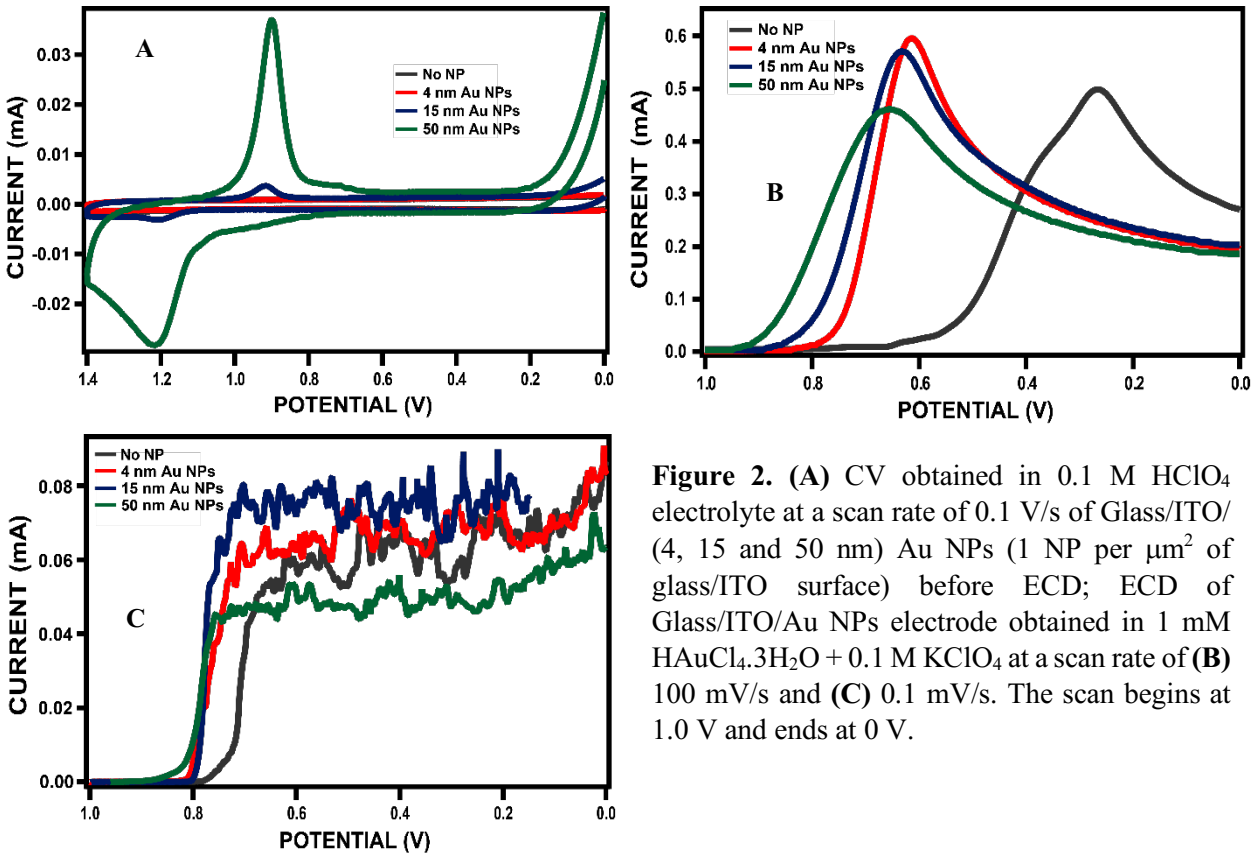

Figure 2. (A) CV obtained in 0.1 M $HClO_4$ electrolyte at a scan rate of 0.1 V/s of Glass/ITO/ (4, 15 and 50 nm) Au NPs (1 NP per μm^2 of glass/ITO surface) before ECD; ECD of Glass/ITO/Au NPs electrode obtained in 1 mM $HAuCl_4.3H_2O$ + 0.1 M $KClO_4$ at a scan rate of **(B)** 100 mV/s and **(C)** 0.1 mV/s. The scan begins at 1.0 V and ends at 0 V.

Interestingly, the peak currents are still slightly larger for the smaller Au NPs, even though they exhibited higher overpotential for ECD. The peak currents were 6.11 x 10^{-4} A, 5.09 x 10^{-4} A, and 3.60 x 10^{-4} A for the 4 nm, 15 nm, and 50 nm Au NPs, respectively. With linear diffusion at all electrodes, the peak currents should theoretically be the same, proportional to the entire glass/ITO electrode area. When we decreased the scan rate to 0.1 mV/s at Au NP coverages of 1 NP/μm^2 (Figure 2C), the ECD showed electrochemically reversible kinetics with a growth potential ($E_{1/2}$) of ~0.80 V in all cases and limiting currents. The limiting current for growth was again slightly smaller for the 50 nm Au NPs compared to 4 nm and 15 nm Au NPs.

Coverage-Dependent ECD. The ECD results in Figures 1 and 2 interestingly show that 4 nm Au NPs display faster kinetics per Au surface area compared to larger Au NPs while the larger Au NPs display faster kinetics per NP compared to smaller Au NPs, due to higher surface area per larger NP. In order to investigate the coverage dependence further we studied the ECD for each size Au NPs as a function of coverage in terms of surface area and number of NPs per μm^2. Figure 3 shows the LSVs of 4 nm, 15 nm, and 50 nm Au NPs as a function of coverage at 100 mV/s as indicated in Figures 3A, 3B and 3C, respectively. For all sizes, the peak ECD growth potential shifts positive as the coverage increases. Since the lowest coverage of Au NPs in the range of coverages has NP spacings close enough for diffusional overlap (linear diffusion) at this scan rate, the lack of electrochemical reversibility shows that the electron transfer kinetics are not able to keep up with mass transfer of $AuCl_4^-$ to the electrode surface. Increasing the coverage of Au NPs increases the active area for electron transfer, which allows the electron transfer kinetics to keep up better with mass transfer. The electrochemical reversibility improves with increasing Au NP coverage. It has been observed that the overpotentials due to a catalytic process for surface-attached NP catalysts depends on the SA coverage of the catalytic sites present at the electrode

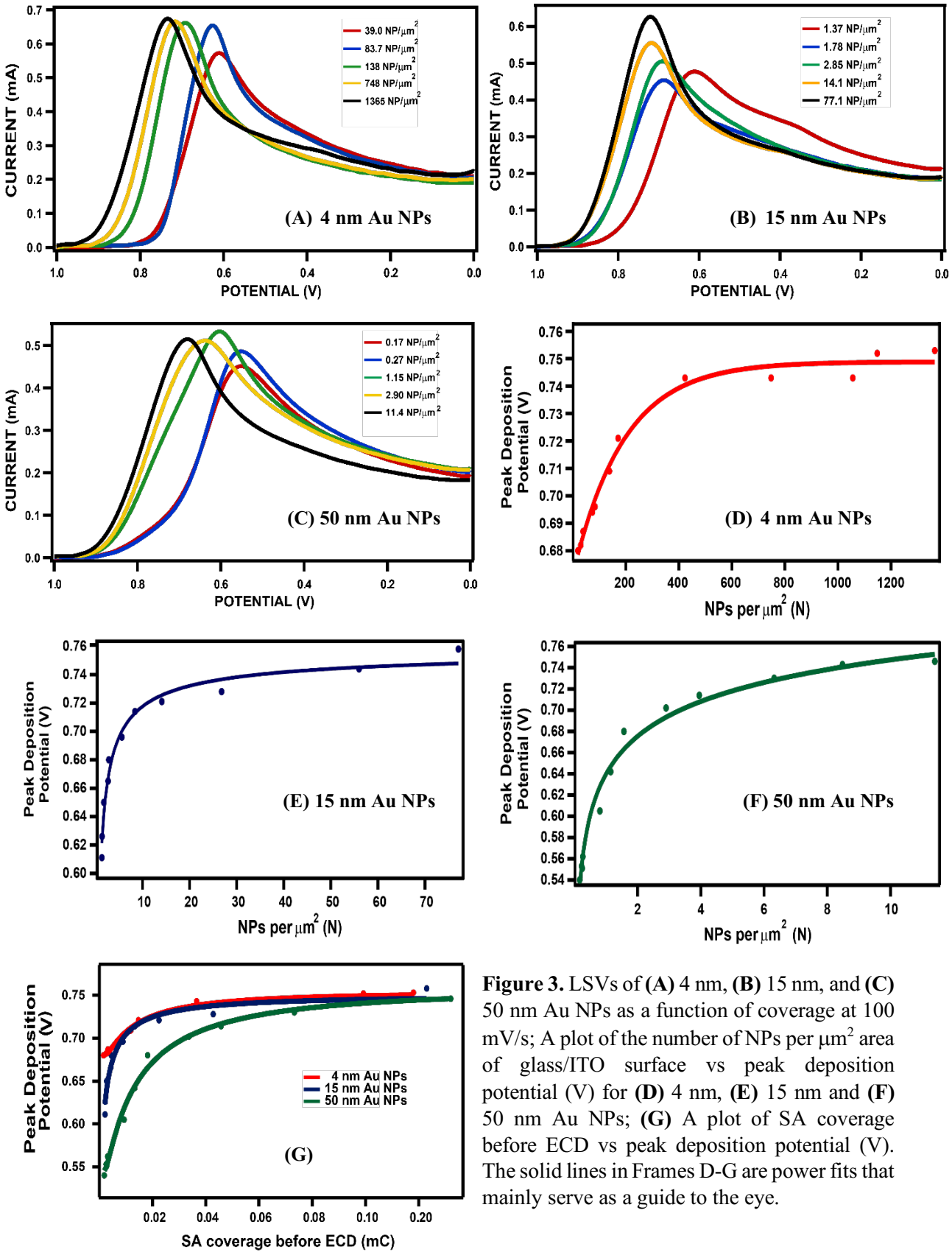

Figure 3. LSVs of **(A)** 4 nm, **(B)** 15 nm, and **(C)** 50 nm Au NPs as a function of coverage at 100 mV/s; A plot of the number of NPs per μm^2 area of glass/ITO surface vs peak deposition potential (V) for **(D)** 4 nm, **(E)** 15 nm and **(F)** 50 nm Au NPs; **(G)** A plot of SA coverage before ECD vs peak deposition potential (V). The solid lines in Frames D-G are power fits that mainly serve as a guide to the eye.

surface.[33, 34] Due to different size-dependent electron transfer kinetics, there exists a different threshold coverage of Au NPs needed on the electrode surface to achieve electrochemical reversibility for the ECD of $AuCl_4^-$ onto Au NPs. The threshold in terms of total number of Au NPs is smaller for the larger Au NPs since the larger Au NPs have a larger total surface area per NP. If we use a potential of 740 mV, the in number of NPs is ~400 NPs/μm^2, ~40 NPs/μm^2, and ~8.5 NPs/μm^2 for the 4 nm, 15 nm, and 50 nm Au NPs, respectively (Figure 3D-3F), to reach that peak potential. More importantly, the threshold value occurs at a lower Au total surface area for the 4 nm Au NPs, confirming that the smaller Au NPs have more catalytic activity for ECD of Au per Au surface area, volume, and mass. Figure 3G shows a plot of the growth potential for all three Au NP sizes as a function of total Au surface area (Tables S2-S4). A peak growth potential of ~743 mV corresponds to surface areas of 3.66 x 10^{-5} C, 8.93 x 10^{-5} C, and 9.84 x 10^{-5} C for 4 nm, 15 nm, and 50 nm Au NPs, respectively. The peak deposition potentials reach a plateau with close to reversible kinetics at ~743 mV, indicating that the size dependent behavior diminishes at higher surface area coverages due to reasons already discussed. This shows that the 15 nm and 50 nm Au NPs require ~2-3 times the surface area as 4 nm Au NPs to achieve the same electrochemical reversibility.

Figure 4 shows the ECD of Au on glass/ITO/Au NP electrodes of different size with a total surface area coverage of ~4 x 10^{-6} C. We performed ECD in a solution of 0.1 mM $HAuCl_4.3H_2O$ and 0.1 M $KClO_4$ by sweeping the potential from 1.0 V to 0.0 V vs Ag/AgCl (3 M KCl) at a scan rate of 100 mV/s. Interestingly, with lower concentrations of $AuCl_4^-$, the peak growth potential (~730 mV) does not depend strongly on the size of the Au NPs. With lower $AuCl_4^-$, the number of Au NPs present at the glass/ITO surface is enough to support the flux of $AuCl_4^-$ ions during ECD. The concentration gradient, and hence the flux, is lower when the bulk metal ion complex

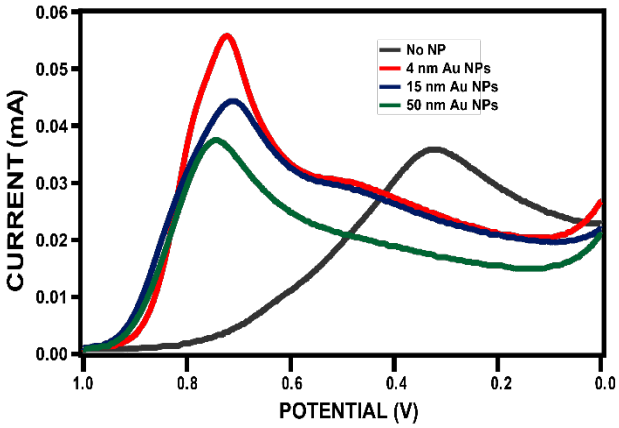

Figure 4. ECD of Glass/ITO/Au NPs (4, 15 and 50 nm) electrodes obtained in 0.1 mM $HAuCl_4.3H_2O$ + 0.1 M $KClO_4$ at a scan rate of 100 mV/s. The scan begins at 1.0 V and ends at 0 V.

concentration decreases. A high $AuCl_4^-$ concentration results in higher flux, or lower mass-transfer resistance, which results in the resistance to electron transfer being the rate limiting step. This causes the kinetic limitations observed at 1 mM concentrations. With a lower concentration of $AuCl_4^-$, the higher mass-transfer resistance is the rate limiting step and we do not observe electron transfer kinetic limitations. This leads to more reversible voltammetry at all NP sizes. The peak currents associated with ECD were 5.59 x 10^{-5} A, 4.08 x 10^{-5} A, and 3.16 x 10^{-5} A for the 4 nm, 15 nm, and 50 nm Au NPs, respectively (Table S5). It is also important to note that the peak growth potential with glass/ITO/Au NPs are more positive by ~500 mV compared to the peak nucleation and growth potential for glass/ITO even with the lower $AuCl_4^-$ concentration. This again shows that the growth step occurs at much lower overpotentials compared to the nucleation step due to much slower nucleation kinetics compared to growth kinetics.

Figure 5 shows a linear sweep voltammogram (LSV) from 1.0 V to 0.0 V (vs. Ag/AgCl) at a scan rate of 100 mV/s of a glass/ITO/15 nm Au NPs electrode with a coverage of 0.60 NPs/μm^2 in a solution of 1 mM $HAuCl_4{\cdot}3H_2O$ and 0.1 M $KClO_4$ (Frame A) and the corresponding SEM image after the LSV (Frame B). Interestingly, the SEM image shows the presence of two particle size populations. There are those that grew greater than about 100 nm (indicated by yellow circles) and those that did not grow very large (indicated by red circles), remaining in the 15 to 50 nm size range. The original coverage of Au NPs based on the the SA from the CV in 0.1 M $HClO_4$ was

about 2.2 NPs/μm^2. The coverage of Au NPs from 6 different SEM images and close to 100 total NPs was 1.4 NPs/μm^2 when including both the larger and smaller Au NPs. Based on the SEM coverage being smaller, we conclude that all the Au NPs in the SEM images originated from 15 nm Au seed NPs that grew during the LSV, but that some of the Au NPs were more active and grew larger than others. This is consistent with the large size dispersity (often bimodal distribution) that is observed with an ensemble of metal NPs growing by ECD under conditions of linear diffusion with overlapping diffusion layers.[26] We will report on more detailed SEM imaging of different sized Au NPs after growth at different ECD potentials over time in a future investigation.

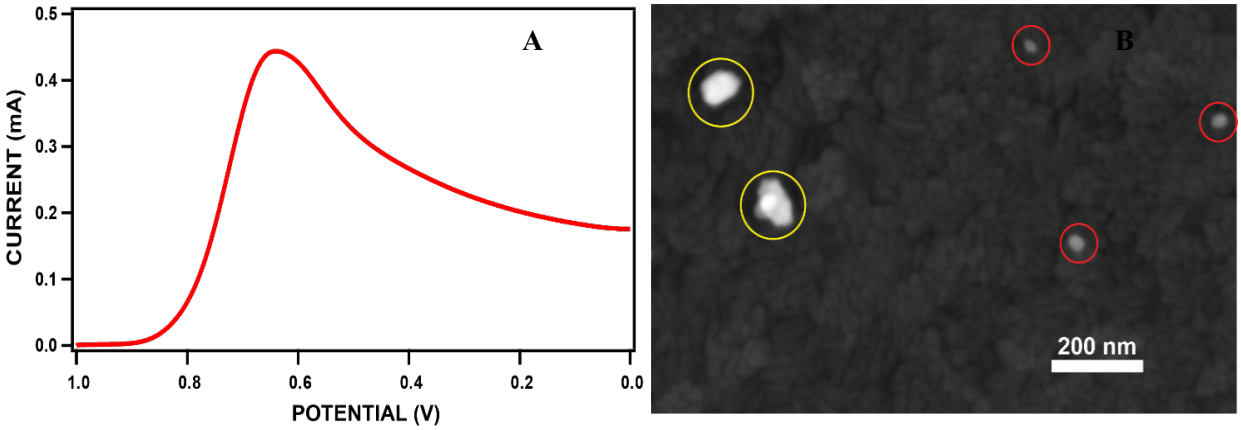

Figure 5. (A) ECD of Glass/ITO/15 nm Au NPs electrodes (0.604 NP/μm^2) in 1 mM $HAuCl_4.3H_2O$ + 0.1 M $KClO_4$ at a scan rate of 100 mV/s. The scan begins at 1 V and ends at 0 V; **(B)** SEM images of Glass/ITO/15 nm Au NPs electrodes after ECD, yellow circles indicate the grown particles and red circle indicate the particles that didn't grow after ECD.

CONCLUSIONS

In summary, we describe the ECD of metallic Au from $AuCl_4^-$ precursor ions onto different sized Au NPs attached to glass/ITO electrodes by EPD. When the scan rate was 100 mV/s, the peak ECD potential increases positive (less overpotential) as the size of the Au NPs decreases provided the overall exposed Au NP surface area is constant. However, when the scan rate is slow ($\leq$ 10 mV/s), the peak ECD potentials become mostly independent of the size of the Au NP. The

peak ECD currents follow a similar trend where it is larger for smaller Au NPs at a scan rate of 100 mV/s when the voltammetry is controlled by the electron transfer kinetics, while at slower scan rates the peak current is very similar for 4 nm and 15 nm Au NPs and a little smaller for 50 nm Au NPs and bare glass/ITO. Another major finding is that the electrochemical reversibility of the process depends on the Au NP coverage. Above a threshold Au surface area, the system displays electrochemical reversible voltammetry for all Au NP sizes. To achieve a peak potential of ~740 mV, 15 nm and 50 nm Au NPs needed ~2-3 times more surface area than 4 nm Au NPs. Similar electrochemical reversibility behavior occurred with ECD using low concentrations of $AuCl_4^-$, showing that the reversibility of the system depends on the $AuCl_4^-$ concentration relative to the Au NP surface area. If the number of catalytic reaction sites present at the electrode surface are enough to keep up with the $AuCl_4^-$ flux as determined by the scan rate and $AuCl_4^-$ bulk concentration, the system is electrochemically reversible. In conclusion, the kinetics of electrochemical growth at Au NP "seeds", or "nucleation sites", is influenced by the size of the NPs presents on the electrode surface, their number density (Au NP total surface area), and $AuCl_4^-$ flux. A better understanding of the details of size- and coverage-dependent Au NP growth by ECD will help researchers better control the growth of metal NPs on electrode surfaces for electrocatalysis, electrochemical sensing, electrosynthesis, and electrooptical applications.

ASSOCIATED CONTENT

Supporting Information. The Supporting Information is available free of charge at https://pubs.acs.org. Table showing electrochemical deposition data for different-sized Au NPs at a coverage of 1 NP/μm^2, tables showing electrochemical deposition data for 4 nm, 15 nm, and 50 nm Au NPs at different coverages, and example calculations for diffusion layer thickness, Au NP coverage, and Au NP-Au NP spacing.

AUTHOR INFORMATION

Corresponding Author

*E-mail: f.zamborini@louisville.edu

ACKNOWLEDGMENTS

We gratefully acknowledge the National Science Foundation (NSF) for financial support of this research through grant CHE-2004169. Thanks to Dr. A. Shoji Hall for helpful discussions about the relationship between catalytic rates and the coverage of catalytic sites.

REFERENCES

(1) Gurrappa, I.; Binder, L. Electrodeposition of Nanostructured Coatings and their Characterization—A Review. *Sci. Technol. Adv. Mater.* **2008**, *9*, 043001-043011.

(2) Andricacos, P. C.; Uzoh, C.; Dukovic, J. O.; Horkans, J.; Deligianni, H. Damascene Copper Electroplating for Chip Interconnections. *IBM J. Res. Dev.* **1998**, *42*, 567-574.

(3) Höltig, M.; Ruhmlieb, C.; Kipp, T.; Mews, A. Highly Efficient Fuel Cell Electrodes from Few-Layer Graphene Sheets and Electrochemically Deposited Palladium Nanoparticles. *J. Phys. Chem. C* **2016**, *120*, 7476-7481.

(4) Wang, Y.; Yu, Y.; Liu, Y.; Yang, S. Template-Confined Site-Specific Electrodeposition of Nanoparticle Cluster-in-Bowl Arrays as Surface Enhanced Raman Spectroscopy Substrates. *ACS Sens.* **2018**, *3*, 2343-2350.

(5) Penner, R. M. A Nose for Hydrogen Gas: Fast, Sensitive H2 Sensors Using Electrodeposited Nanomaterials. *Acc. Chem. Res.* **2017**, *50*, 1902-1910.

(6) Glasscott, M. W.; Pendergast, A. D.; Dick, J. E. A Universal Platform for the Electrodeposition of Ligand-Free Metal Nanoparticles from a Water-in-Oil Emulsion System. *ACS Appl. Nano Mater.* **2018**, *1*, 5702-5711.

(7) Pendergast, A. D.; Glasscott, M. W.; Renault, C.; Dick, J. E. One-Step Electrodeposition of Ligand-Free PdPt Alloy Nanoparticles from Water Droplets: Controlling Size, Coverage, and Elemental Stoichiometry. *Electrochem. Commun.* **2019**, *98*, 1-5.

(8) Li, C.; Iqbal, M.; Lin, J.; Luo, X.; Jiang, B.; Malgras, V.; Wu, K. C.; Kim, J.; Yamauchi, Y. Electrochemical Deposition: An Advanced Approach for Templated Synthesis of Nanoporous Metal Architectures. *Acc. Chem. Res.* **2018**, *51*, 1764-1773.

(9) Ma, R.; Lu, N.; Liu, L.; Wang, Y.; Shi, S.; Chi, L. Fabrication of Single Gold Particle Arrays with Pattern Directed Electrochemical Deposition. *ACS Appl. Mater. Interfaces* **2012**, *4*, 3779-3783.

(10) Tanabe, I.; Tatsuma, T. Size- and Shape-Controlled Electrochemical Deposition of Metal Nanoparticles by Tapping Mode Atomic Force Microscopy. *J. Phys. Chem. C* **2012**, *116*, 3995-3999.

(11) Ivanova, O. S.; Zamborini, F. P. Electrochemical Size Discrimination of Gold Nanoparticles Attached to Glass/Indium-Tin-Oxide Electrodes by Oxidation in Bromide-Containing Electrolyte. *Anal. Chem.* **2010**, *82*, 5844-5850.

(12) Martin, B. R.; Dermody, D. J.; Reiss, B. D.; Fang, M.; Lyon, L. A.; Natan, M. J.; Mallouk, T. E. Orthogonal Self-Assembly on Colloidal Gold-Platinum Nanorods. *Adv. Mater.* **1999**, *11*, 1021-1025.

(13) Cross, C. E.; Hemminger, J. C.; Penner, R. M. Physical Vapor Deposition of One-Dimensional Nanoparticle Arrays on Graphite: Seeding the Electrodeposition of Gold Nanowires. *Langmuir* **2007**, *23*, 10372-10379.

(14) Menke, E. J.; Thompson, M. A.; Xiang, C.; Yang, L. C.; Penner, R. M. Lithographically Patterned Nanowire Electrodeposition. *Nat. Mater* **2006**, *5*, 914-919.

(15) Altimari, P.; Pagnanelli, F. Electrochemical Nucleation and Three-Dimensional Growth of Metal Nanoparticles under Mixed Kinetic-Diffusion Control: Model Development and Validation. *Electrochim. Acta* **2016**, *206*, 116-126.

(16) Lai, S. C. S.; Lazenby, R. A.; Kirkman, P. M.; Unwin, P. R. Nucleation, Aggregative Growth and Detachment of Metal Nanoparticles during Electrodeposition at Electrode Surfaces. *Chem. Sci.* **2015**, *6*, 1126-1138.

(17) Velmurugan, J.; Mirkin, M. V. Fabrication of Nanoelectrodes and Metal Clusters by Electrodeposition. *ChemPhysChem* **2010**, *11*, 3011-3017.

(18) Liu, L.; Zhu, X.; Wei, S.; Zhang, J.; Baklanov, M. R.; Fanta, A. B. d. S.; Niu, J.; Xie, C. Influence of Current Density on Orientation-Controllable Growth and Characteristics of Electrochemically Deposited Au Films. *J. Electrochem. Soc.* **2018**, *166*, D3232-D3237.

(19) Jana, N. R.; Gearheart, L.; Murphy, C. J. Wet Chemical Synthesis of High Aspect Ratio Cylindrical Gold Nanorods. *J. Phys. Chem. B* **2001**, *105*, 4065-4067.

(20) Abdelmoti, L. G.; Zamborini, F. P. Potential-Controlled Electrochemical Seed-Mediated Growth of Gold Nanorods Directly on Electrode Surfaces. *Langmuir* **2010**, *26*, 13511-13521.

(21) Fratini, E.; Girella, A.; Saldan, I.; Milanese, C.; Dobrovetska, O.; Sus, L.; Okhremchuk, Y.; Kuntyi, O.; Reshetnyak, O. Nucleation and Growth of Au And Au–Pd Nanoparticles at the Beginning of Electrochemical Deposition. *Mater. Lett.* **2015**, *161*, 263-266.

(22) Wu, S.; Yin, Z.; He, Q.; Lu, G.; Yan, Q.; Zhang, H. Nucleation Mechanism of Electrochemical Deposition of Cu on Reduced Graphene Oxide Electrodes. *J. Phys. Chem. C* **2011**, *115*, 15973-15979.

(23) Ustarroz, J.; Altantzis, T.; Hammons, J. A.; Hubin, A.; Bals, S.; Terryn, H. The Role of Nanocluster Aggregation, Coalescence, and Recrystallization in the Electrochemical Deposition of Platinum Nanostructures. *Chem. Mater.* **2014**, *26*, 2396-2406.

(24) Venkatasubramanian, R.; Jin, K.; Pesika, N. S. Use of Electrochemical Deposition to Create Randomly Rough Surfaces and Roughness Gradients. *Langmuir* **2011**, *27*, 3261-3265.

(25) Hussein, H. E. M.; Maurer, R. J.; Amari, H.; Peters, J. J. P.; Meng, L.; Beanland, R.; Newton, M. E.; Macpherson, J. V. Tracking Metal Electrodeposition Dynamics from Nucleation and Growth of a Single Atom to a Crystalline Nanoparticle. *ACS Nano* **2018**, *12*, 7388-7396.

(26) Penner, R. Brownian Dynamics Simulations of the Growth of Metal Nanocrystal Ensembles on Electrode Surfaces in Solution: 2. The Effect of Deposition Rate on Particle Size Dispersion. *J. Phys. Chem. B* **2001**, *105*, 8672-8678.

(27) Allen, S. L.; Zamborini, F. P. Size-Selective Electrophoretic Deposition of Gold Nanoparticles Mediated by Hydroquinone Oxidation. *Langmuir* **2019**, *35*, 2137-2145.

(28) Masitas, R. A.; Allen, S. L.; Zamborini, F. P. Size-Dependent Electrophoretic Deposition of Catalytic Gold Nanoparticles. *J. Am. Chem. Soc.* **2016**, *138*, 15295-15298.

(29) Sharma, J. N.; Pattadar, D. K.; Mainali, B. P.; Zamborini, F. P. Size Determination of Metal Nanoparticles Based on Electrochemically Measured Surface-Area-to-Volume Ratios. *Anal. Chem.* **2018**, *90*, 9308-9314.

(30) Guo, L.; Searson, P. C. On the Influence of the Nucleation Overpotential on Island Growth in Electrodeposition. *Electrochim. Acta* **2010**, *55*, 4086-4091.

(31) Altimari, P.; Greco, F.; Pagnanelli, F. Nucleation and Growth of Metal Nanoparticles on a Planar Electrode: A New Model Based on Iso-Nucleation-Time Classes of Particles. *Electrochim. Acta* **2019**, *296*, 82-93.

(32) Oskam, G.; Searson, P. C. Electrochemical Nucleation and Growth of Gold on Silicon. *Surf. Sci.* **2000**, *446*, 103-111.

(33) Ferreira, P. J.; la O', G. J.; Shao-Horn, Y.; Morgan, D.; Makharia, R.; Kocha, S.; Gasteiger, H. A. Instability of Pt/C Electrocatalysts in Proton Exchange Membrane Fuel Cells: A Mechanistic Investigation. *J. Electrochem. Soc.* **2005**, *152*, A2256-A2271.

(34) Zhang, J.; Sasaki, K.; Sutter, E.; Adzic, R. R. Stabilization of Platinum Oxygen-Reduction Electrocatalysts Using Gold Clusters. *Science* **2007**, *315*, 493-497.

TOC GRAPHIC